Journal of Applied Geophysics 110 (2014) 5–22

Contents lists available at ScienceDirect

Journal of Applied Geophysics

journal homepage: www.elsevier.com/locate/jappgeo

River embankment characterization: The joint use of geophysical and geotechnical techniques

Maria Teresa Perri [a,*], Jacopo Boaga [a], Silvia Bersan [b], Giorgio Cassiani [a], Simonetta Cola [b], Rita Deiana [c], Paolo Simonini [b], Salvatore Patti [d]

[a] Dipartimento di Geoscienze, Università degli Studi di Padova, Padua, Italy
[b] Dipartimento di Ingegneria Civile Edile ed Ambientale (DICEA), Università degli Studi di Padova, Padua, Italy
[c] Dipartimento dei Beni Culturali: archeologia, storia dell'arte, del cinema e della musica, Università degli Studi di Padova, Padua, Italy
[d] Ufficio del Genio Civile di Venezia, Venice, Italy

ARTICLE INFO

Article history:
Received 29 December 2013
Accepted 25 August 2014
Available online 1 September 2014

Keywords:
ERT
FDEM
GPR
Embankment monitoring
Flood risk mitigation

ABSTRACT

Recent flood events in Northern Italy (particularly in the Veneto Region) have brought river embankments into the focus of public attention. Many of these embankments are more than 100 years old and have been repeatedly repaired, so that detailed information on their current structure is generally missing. The monitoring of these structures is currently based, for the most part, on visual inspection and localized measurements of the embankment material parameters. However, this monitoring is generally insufficient to ensure an adequate safety level against floods. For these reasons there is an increasing demand for fast and accurate investigation methods, such as geophysical techniques. These techniques can provide detailed information on the subsurface structures, are non-invasive, cost-effective, and faster than traditional methods. However, they need verification in order to provide reliable results, particularly in complex and reworked man-made structures such as embankments. In this paper we present a case study in which three different geophysical techniques have been applied: electrical resistivity tomography (ERT), frequency domain electromagnetic induction (FDEM) and Ground Penetrating Radar (GPR). Two test sites have been selected, both located in the Province of Venice (NE Italy) where the Tagliamento River has large embankments. The results obtained with these techniques have been calibrated against evidence resolving from geotechnical investigations. The pros and cons of each technique, as well as their relative merit at identifying the specific features of the embankments in this area, are highlighted. The results demonstrate that geophysical techniques can provide very valuable information for embankment characterization, provided that the data interpretation is constrained via direct evidence, albeit limited in space.

1. Introduction

The dramatic flood events that occurred in North-Eastern Italy, and particularly in the Veneto Region, in November 2010 highlighted the extreme vulnerability that characterizes the local river embankments, and the pressing need for a system allowing a better control of these structures. A proper characterization of levees and their foundation layers is, in general, one of the main tools for flood risk mitigation. This risk is due to the exceptional changes in the water levels that follow intense precipitation events and can cause the collapse of the levee system. The mechanisms of embankment collapse, which involve both the streamside and the landside slopes (as well as the foundation layer), are linked to the change in the hydraulic regime of river flow. For example, high water levels – prolonged in time – may gradually lead to saturation of the containment structures, reducing their resistance. Conversely, a rapid lowering of the water level, such as those occurring in the descent phase of an overflow, can cause the development of dangerous filtration forces towards the streamside.

The heterogeneity in the grain size and hydraulic properties of the soil composing the embankment and its foundation can lead to the formation of preferential seepage pathways and/or the removal of soil particles ultimately leading to collapse (internal erosion). Erosion can also occur in discontinuities along rigid structures embedded in the levee. Burrows excavated by animals such as beavers and nutrias are also dangerous triggers for internal erosion.

In practice, the processes described above are not easily detectable, as they evolve without any superficial evidence until the collapse of the levee system. As embankment monitoring is, in fact, currently based on visual inspection and localized measurements (e.g. using piezometers) of the soil parameters, it is hardly surprising that the standard monitoring is insufficient to ensure an adequate safety level.

* Corresponding author at: Dipartimento di Geoscienze, Università degli Studi di Padova, Padova, via Gradenigo 6, 35131, Italy. Tel.: +39 338 6251593 (Mob); fax: +39 049 8279134.
E-mail addresses: mariateresa.perri@unipd.it (M.T. Perri), jacopo.boaga@unipd.it (J. Boaga), bersan.vr@gmail.com (S. Bersan), giorgio.cassiani@unipd.it (G. Cassiani), simonetta.cola@unipd.it (S. Cola), rita.deiana@unipd.it (R. Deiana), paolo.simonini@unipd.it (P. Simonini).

http://dx.doi.org/10.1016/j.jappgeo.2014.08.012
0926-9851/

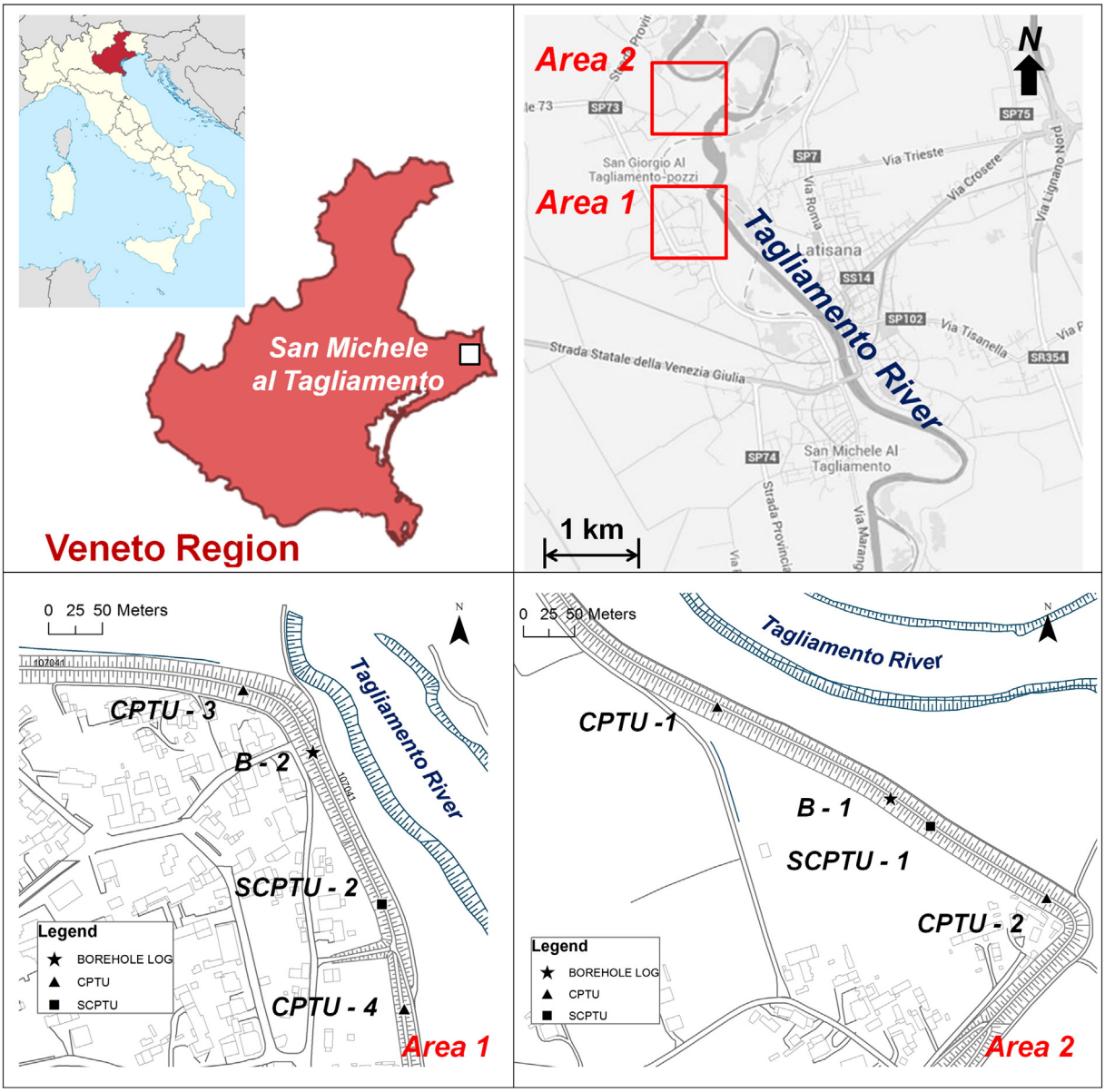

Fig. 1. Test sites (*Area 1* and *Area 2*) near San Michele al Tagliamento, in the Veneto Region (Province of Venice, North-Eastern Italy). In situ geotechnical tests are indicated by black symbols: the stars denote the location of boreholes, the triangles indicate the location of CPTU tests and the squares that of the SCPTU tests. Maps from Google Maps and Wikipedia, successively modified.

This is the reason why the demand for fast and extensive, while still informative, investigation methods is rapidly increasing. Geophysical techniques can be a viable choice, as they are sensitive to soils/rocks physical properties and variables which, in turn, are related to grain size, porosity, water content, and temperature (Reynolds, 2011). These soil properties and state variables can hence provide information about subsurface characteristics and can be particularly useful in locating subsurface features of geotechnical and engineering interest. Furthermore, these methods can cover large portions of the investigated system, often with meter resolution, in relatively short time.

The recent scientific literature shows that the most used techniques for embankment characterization are: electrical resistivity tomography – ERT – (Buselli and Lu, 2001; Cho and Yeom, 2007; Fauchard and Meriaux, 2007; Inazaki, 2007; Niederleithinger et al., 2012; Panthulu et al., 2001; Voronkov et al., 2004), electromagnetic surveys – EM – (Fauchard and Meriaux, 2007; Inazaki, 2007; Niederleithinger et al., 2012) and Ground Penetrating Radar – GPR – (Biavati et al., 2008; Di Prinzio et al., 2010; Fauchard and Meriaux, 2007; Niederleithinger et al., 2012; Szynkiewicz, 2000). However, the number of case studies where different techniques are compared with each other and with direct investigations is very limited and there is a lack of information on the selection of suitable procedures and measurement parameters.

The goal of this paper is to present a case study where the joint use of several geophysical techniques and of geotechnical methods permits a solid analysis of advantages and disadvantages of each method. The experimental area is located at San Michele al Tagliamento (Province of Venice, Italy) and the activity was focused on the local embankments of the Tagliamento River. In this paper we analyze the influence of subsoil conditions on measurement results and the different investigation capabilities of the adopted methods. As the comparison with direct techniques (invasive) is necessary to calibrate and validate the results obtained with the geophysical measurements, we used an integrated approach linking invasive (geotechnical) and non-invasive techniques. The joint analysis of all data allows for solid conclusions to be drawn for the specific case study, but is also presented here as a proposed general approach for embankment characterization.

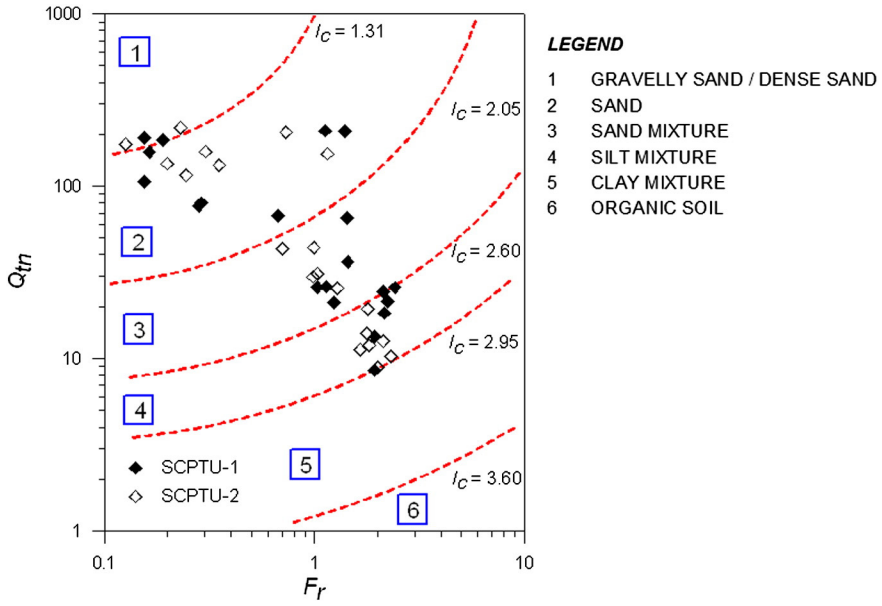

Fig. 2. Classification chart according to Soil Behavior Type index (I_c) calculated from CPTU data.

2. Case study and methodology

The considered experimental site lies in the municipality of San Michele al Tagliamento, in the province of Venice (Fig. 1). From a geological point of view, the site is located in the lower plain of the Tagliamento River, characterized by the presence of alluvial sediments deposited by the river from the Last Glacial Maximum (30,000 to 17,000 years B. P.) to Present. In particular, two main stratigraphic units can be distinguished: (1) the Spilimbergo Sintema (Late Pleistocene), related to the phase of glacier advancement during the Last Glacial Maximum and consisting of fine to medium sands with lenses of silts and clayey silts and, secondly, of gravelly sands and sand with layers of silt and clay; (2) the Po Sintema (Late Pleistocene–Holocene), that is formed by a first unit of sandy gravels and sand alternated with silty layers and a second unit of fine sands alternated with silts, sandy silts and clayey silts (Fontana et al., 2012).

The Tagliamento River has a pluvio-nival hydrologic regime, with frequent flash floods and flow pulses that generally occur in spring and autumn. Due to the steep slopes and the strong erosion processes in the upper catchment (placed in the Carnian and Julian Alps), very intense rainstorms may generate massive flow and sediment transport rates (Tockner et al., 2003). This is the reason why in the lower plain, where densely populated areas are present and the risk is more severe, a continuous system of earthen levees was erected more than a century ago to contain river during flood stages. The material used for the embankments was generally taken from the river bed and the floodplain.

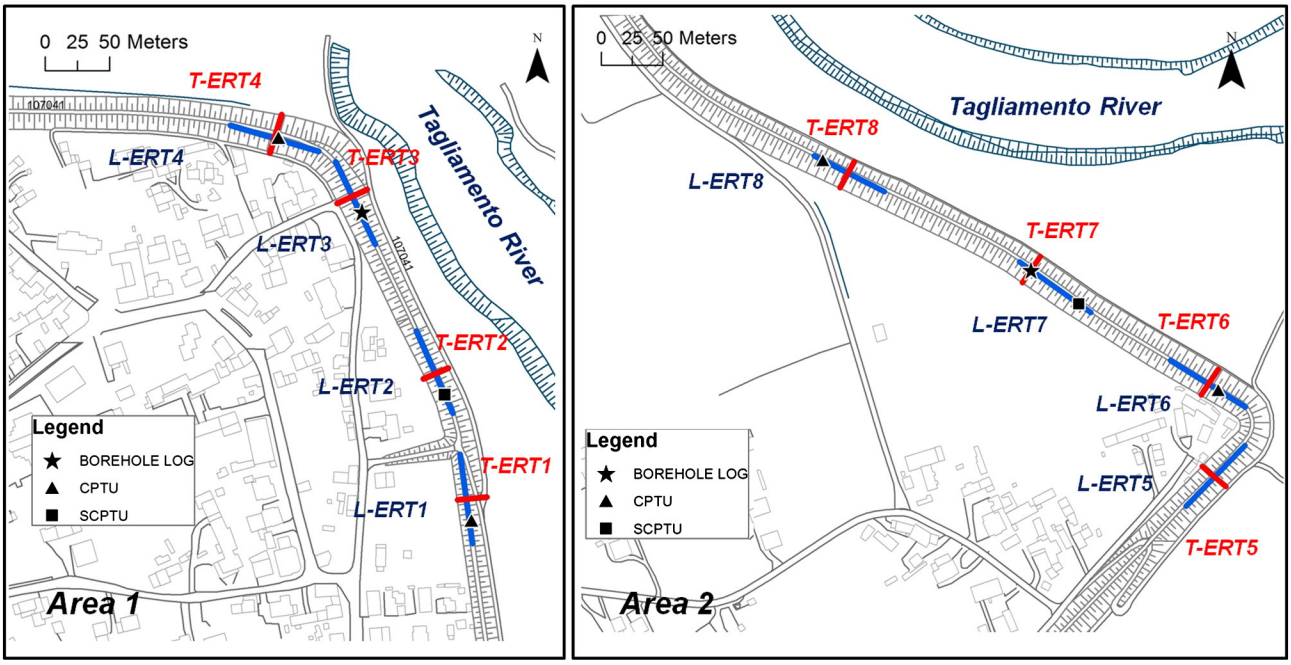

Fig. 3. ERT surveys conducted on the levee crest in Area 1 and Area 2. The longitudinal profiles are labeled from L-ERT1 to 4 in Area 1 and from L-ERT5 to 8 in Area 2; the transverse profiles are labeled from T-ERT1 to 4 in Area 1 and from T-ERT5 to 8 in Area 2.

As the levees have been repeatedly repaired during the time, their internal structure is likely to be heterogeneous both in lateral and longitudinal directions, and is practically unknown.

In order to obtain a valid characterization of the Tagliamento River embankments near San Michele al Tagliamento, we carried out several geophysical surveys in two areas, hereinafter referred to as *Area 1*, in the southern part of the pilot site, and *Area 2*, in the northern part (Fig. 1). These areas have been selected for the geophysical experiments as several geotechnical investigations had been previously conducted in the same areas (see Fig. 1 for their locations in the two test sites) and independent information was hence available.

2.1. Geotechnical investigation

The geotechnical in-situ investigations included, for each area, the execution of two piezocone tests (CPTU), one piezocone test with measurement of shear wave velocity (SCPTU) and one borehole (referred to for each site as B-1 and B-2) with core retrieval. Note that the CPTU/SCPTU represents a development of the original cone penetration test (CPT), customarily and extensively used in many site investigations carried out in soils belonging to the classes ranging from sands to clays. The CPTU/SCPTU is performed pushing a cylindrical penetrometer with a conical tip into the ground at a constant rate. During penetration, the forces acting on the cone tip and on the shaft behind the tip are measured. In our case the standard Dutch cone (60° apex angle and base area of 10 cm^2) provided with a pore pressure transducer located on the shaft (Torstensson, 1975) was used. In addition, two geophones installed along the shaft behind the tip and spaced by 1.0 m were used to perform downhole tests that measure shear wave velocity (Tanaka et al., 1994).

Positioning and labeling of the tests are shown in Fig. 1. All investigations reached a depth of around 20 m from the crest of the dike, i.e. around 15 m from ground level on landside.

Calibration of the CPT/CPTU/SCPTU with data from one or more borehole logs is always recommended. For low risk projects CPT/CPTU/SCPTU and index testing on disturbed samples combined with conservative design criteria are often appropriate (Robertson, 2012). The CPT/CPTU/SCPTU has major advantages over traditional methods of field site investigation such as drilling and sampling since it is fast and economical. This allows for the execution of numerous tests if compared to traditional drilling, thus providing reliable information on the spatial variability of the stratigraphic profile. In addition, the continuous nature of the CPTU results provide valuable information about soil variability along depth, that is difficult to match with sampling and laboratory testing. Moreover, the data interpretation has a strong theoretical background (Teh and Houlsby, 1991).

For a fast and direct soil classification by means of CPTU data, few simple rules can be followed. Coarse soils show moderate to high (between 2 and 30 MPa) and highly variable cone resistance while fine grained soils show cone resistances lower than 2 MPa and relatively uniform. The pore water pressures measured during penetration follow the hydrostatic distribution in coarse soils while they strongly increase with respect to the hydrostatic distribution when the cone tip passes through fine grained soil layers. This is due to the undrained/partially drained mechanical response of fine grained soil during cone penetration, that is a function of grain size distribution and stress history (e.g. Cortellazzo and Simonini, 2001). Please note that the pore water pressure readings are fully meaningful only below the water table but give some indications also in the capillary fringe, that extends up to few meters above the water table in clayey materials.

Besides this qualitative information, soil classification is typically accomplished using the friction ratio R_f (Begemann, 1965) or charts that link cone parameters to soil type. Robertson (1990) suggested the term 'soil behavior type' (SBT), because the cone responds to the in-situ mechanical behavior of the soil (e.g. strength, stiffness and compressibility) and not directly to soil classification criteria using geologic descriptors as grain-size distribution and soil plasticity. However there is often good agreement between USCS-based and CPT-based classification.

Robertson (2009) recently defined a Soil Behavior Type (SBT) index, I_c, that depends on the stress-normalized variables Q_{tn} and F_r according to the following expressions:

$$I_c = \sqrt{(3.47 - \log Q_{tn})^2 + (\log F_r + 1.22)^2} \quad (1)$$

$$Q_{tn} = \frac{q_t - \sigma_{v0}}{p_a} \cdot \left(\frac{p_a}{\sigma'_{v0}}\right)^n \quad (2)$$

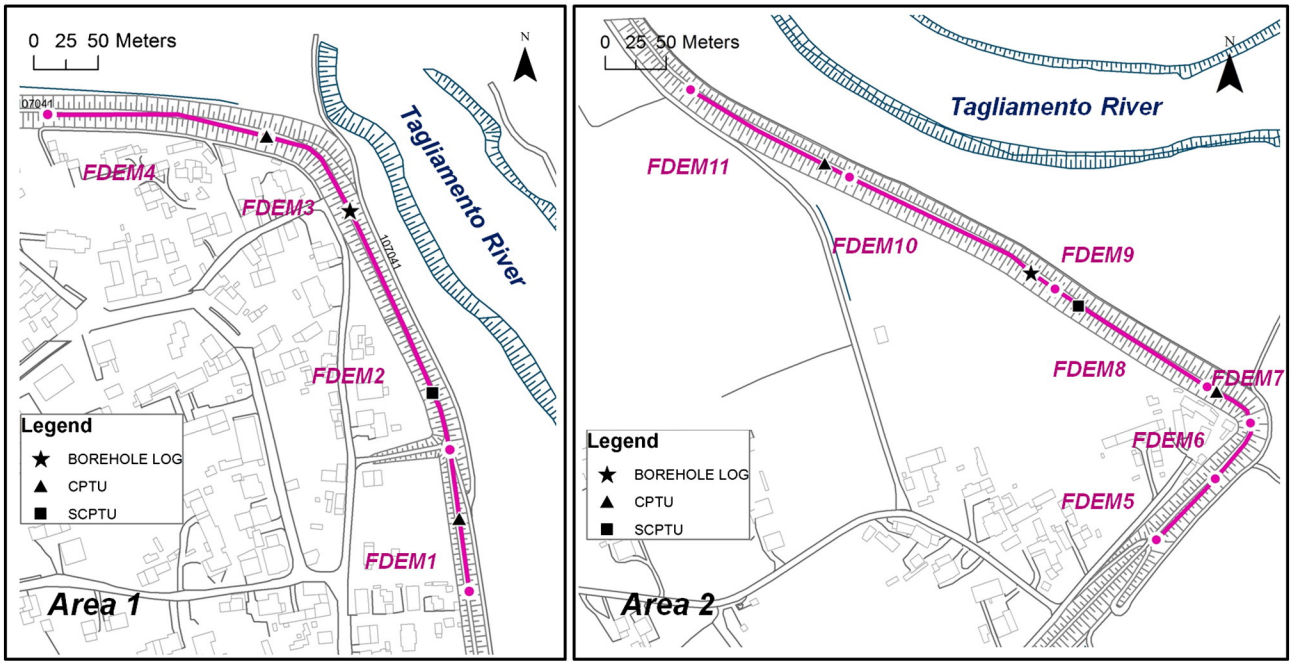

Fig. 4. FDEM surveys conducted on the levee crest in Area 1 and Area 2 test sites. The profiles are labeled from FDEM1 to 4 in Area 1 and from FDEM5 to 11 in Area 2.

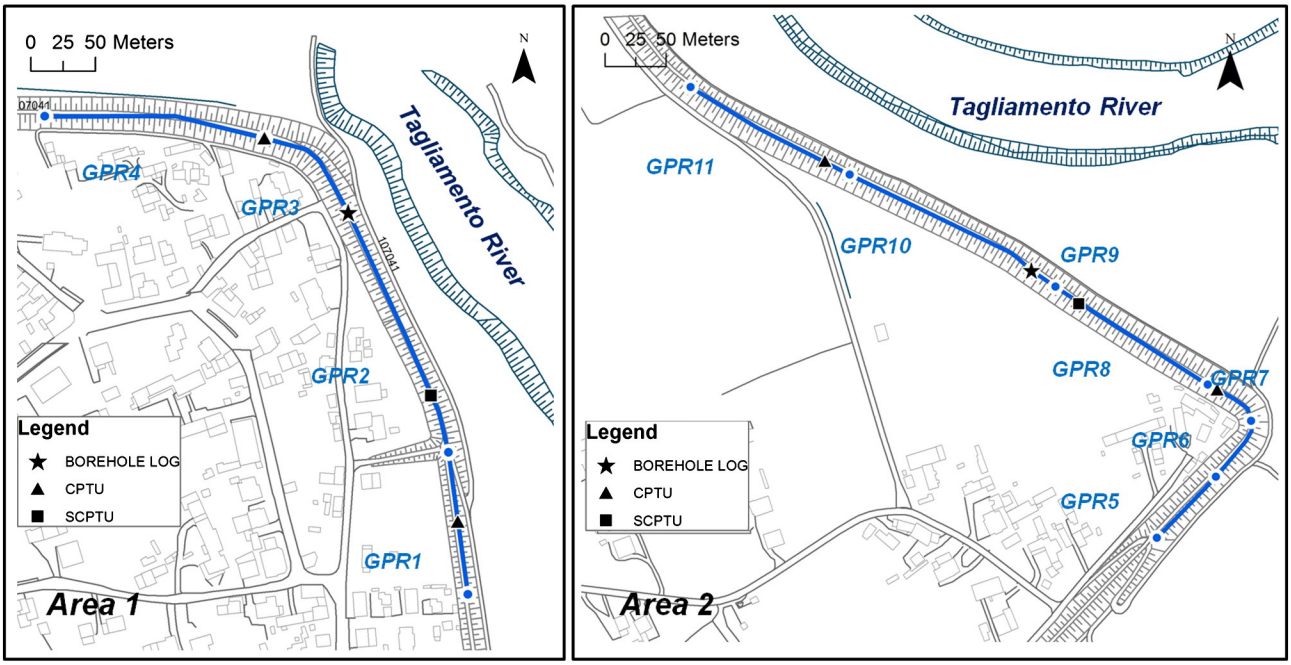

Fig. 5. GPR surveys conducted on the levee crest in Area 1 and Area 2 test sites. The profiles are labeled from GPR1 to GPR4 in Area 1 and from GPR5 to GPR11 in Area 2.

$$F_r = \frac{f_s}{q_t - \sigma'_{v0}} 100\% \quad (3)$$

where σ_{v0} and σ'_{v0} are respectively the total and effective vertical stress and p_a is the atmospheric pressure. The stress exponent n (≤ 1) in Eq. (2) depends on both stress level and SBT index itself:

$$n = 0.38 I_c + 0.05\left(\frac{\sigma'_{v0}}{p_a}\right) - 0.15. \quad (4)$$

In the Q_{tn}–F_r chart, I_c is essentially the radius of concentric circles that define the boundaries of soil type (Fig. 2). A major advantage of the index I_c with respect to traditional charts is that a continuous profile of soil type with depth can be drawn (see e.g. Fig. 8 below).

2.2. Geophysical investigation

We performed a number of geophysical investigations in the same areas investigated with geotechnical methods. These investigations included electrical resistivity tomography (ERT), electromagnetic surveys in the frequency domain (FDEM) and Ground Penetrating Radar (GPR). Overall, these methods are designed to produce an image of the investigated subsurface in terms of electrical conductivity

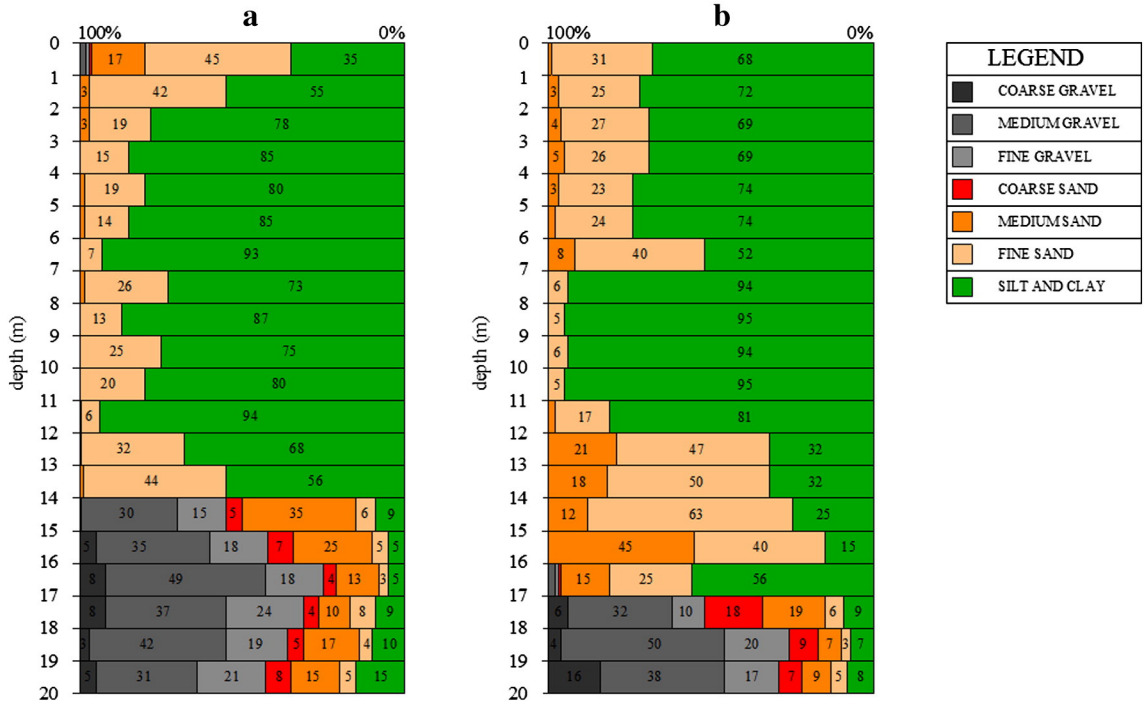

Fig. 6. Borehole logs obtained in the test areas. In particular: borehole B-1 (*a*) has been drilled in Area 2, in the northern part of the test site; borehole B-2 (*b*) has been drilled in Area 1, in the southern part. See Fig. 1 for their location of the map.

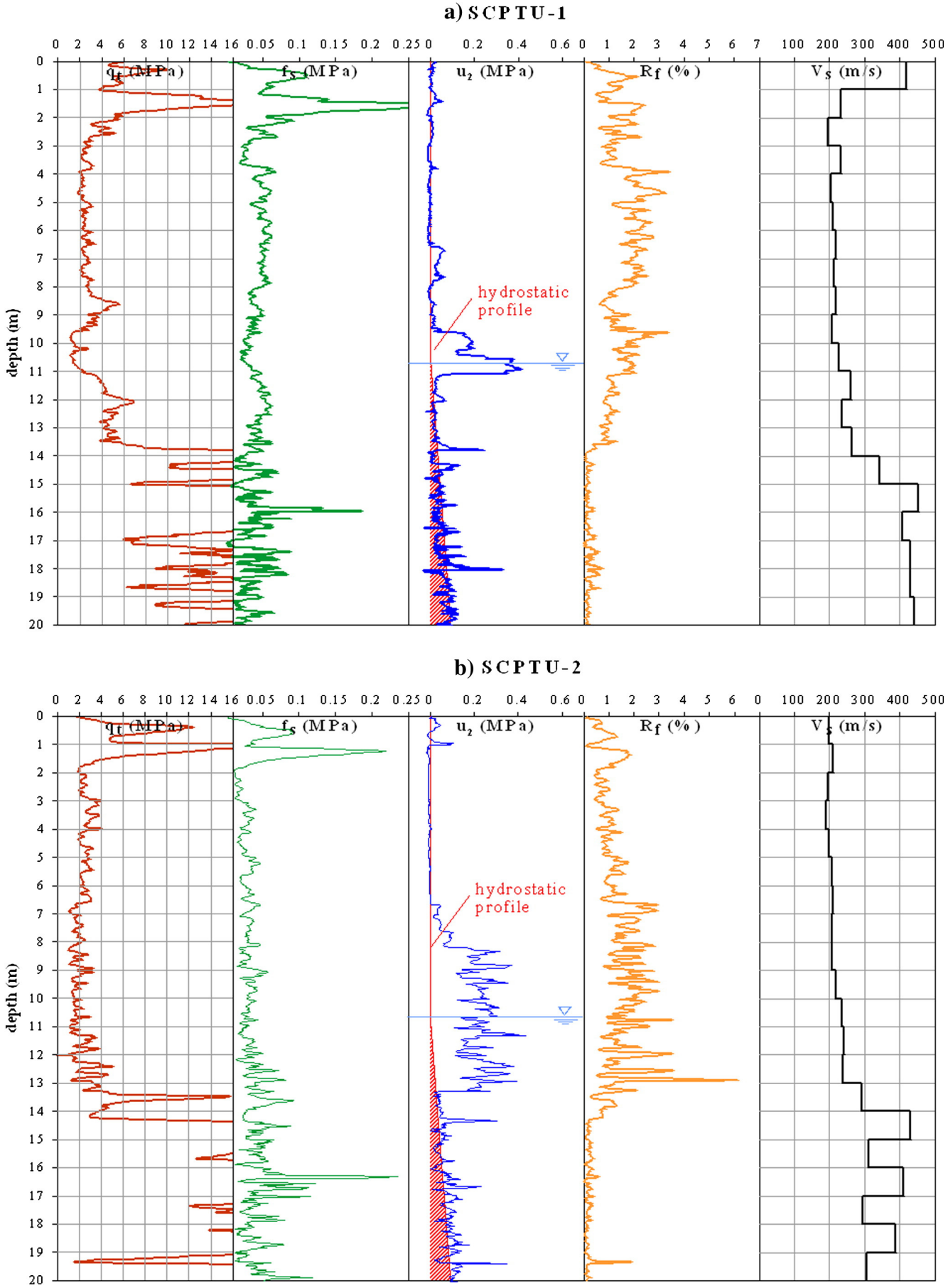

Fig. 7. Results of SCPTU-1 and SCPTU-2 tests conducted respectively in Area 2 and Area 1.

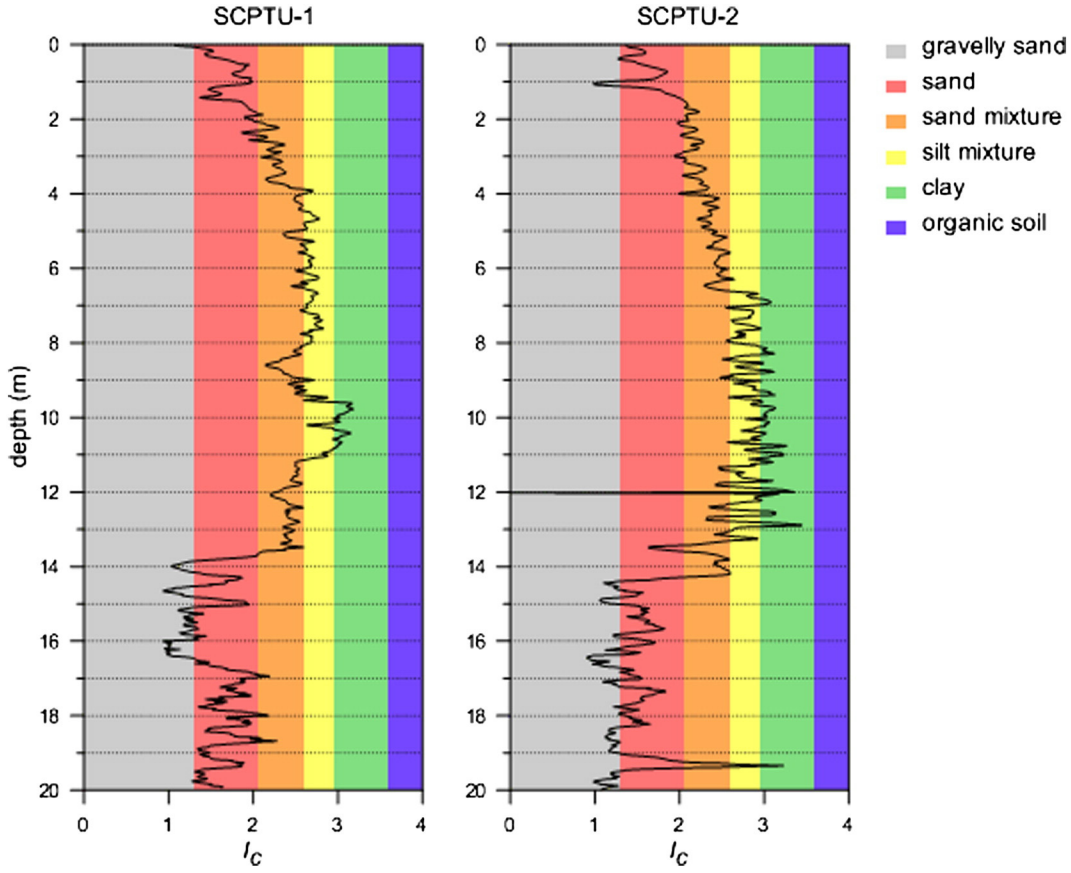

Fig. 8. Continuous profile of Soil Behavior Type index (I_c) calculated from the SCPTU data.

(ERT and FDEM) and dielectric constant (GPR — whose penetration depends on the electrical conductivity of the system), which are strongly related to subsurface lithology and water content.

These methodologies differ in survey resolution, as well as operating modes, that make them more or less suitable for fast site characterization. The FDEM and GPR methods, in particular, do not require any direct contact with the ground and therefore are better suited to cover large areas in a relatively short time; the ERT technique, on the other hand, requires a galvanic contact with the surface and thus longer operating times, but offers a higher resolution and a greater control over signal penetration as compared to FDEM and GPR.

Fig. 3 shows in detail the locations of ERT measurements conducted in San Michele al Tagliamento. The surveys were conducted on the on the levee crests and consisted of:

- eight longitudinal profiles labeled from L-ERT1 to L-ERT4 in Area 1 and from L-ERT5 to L-ERT8 in Area 2, each with 48 electrodes, spaced 1.5 m, for a total length of 70.5 m each and a maximum depth of investigation of about 14 m (computed, as a rule of thumb, as 1/5 of the line length);
- eight transverse profiles, labeled from T-ERT1 to T-ERT4 in Area 1 and from T-ERT5 to T-ERT8 in Area 2, again with 48 electrodes each, spaced 0.5 m, for a total length of 23.5 m for each line and a maximum depth of investigation of slightly less than 5 m. The only exception is represented by T-ERT1 which, due to logistic problems, includes only 24 electrodes spaced 1 m.

For these acquisitions we used an IRIS Instruments Syscal Pro resistivimeter. For each ERT acquisition we adopted a complete dipole–dipole skip zero scheme (i.e. all current and potential dipoles have spacing equal to the minimum electrode separation) that ensures maximal resolution while maintaining, given the short distance at play, a sufficient signal to noise ratio. In order to obtain an estimate of the measurement error, the data were acquired both in direct and in reciprocal mode, i.e. reversing the potential electrodes with current electrodes for each measurement (Daily et al., 2004). The estimation of the data quality is very important because when a regularized least squares inversion (an Occam type inversion) is used, as in this case, the model prediction depends on quantitative estimate of the error level (LaBrecque et al., 1996). In this case study, an error equal to 5% has been considered as a threshold above which data are to be rejected, and the corresponding error level was set as target for the inversion. The data have been inverted using the code *ProfileR* (A. Binley, Lancaster University, UK), an inverse solution for a 2-D resistivity distribution based on computation of 3-D current flow using a quadrilateral finite element mesh.

The survey scheme here chosen allowed to obtain a representative image (in terms of electrical resistivity) of the entire river embankments, which have a height of about 5 m above the natural ground level. It should be emphasized that the results obtained by the longitudinal sections are physically less significant if compared to those obtained by the transverse acquisitions. Only in the second case, in fact, the boundary condition of lateral homogeneity of the medium (thus giving rise to a true 2D resistivity field) is respected. Anyway, the longitudinal acquisitions may still be considered qualitatively informative of the embankment structure (while the resistivity values may be altered by the geometrical configuration).

As far as FDEM is concerned, we acquired a total of eleven profiles, labeled from FDEM1 to FDEM4 in Area 1 and from FDEM5 to FDEM11 in Area 2 (Fig. 4). Note that FDEM is acquired continuously, and this separation into profiles is only given here for convenience of presentation. The data have been acquired using a GF Instruments CMD 4 conductivity meter, using the high depth mode configuration (i.e. with vertical orientation of dipoles) with a nominal maximum depth of investigation of 6 m.

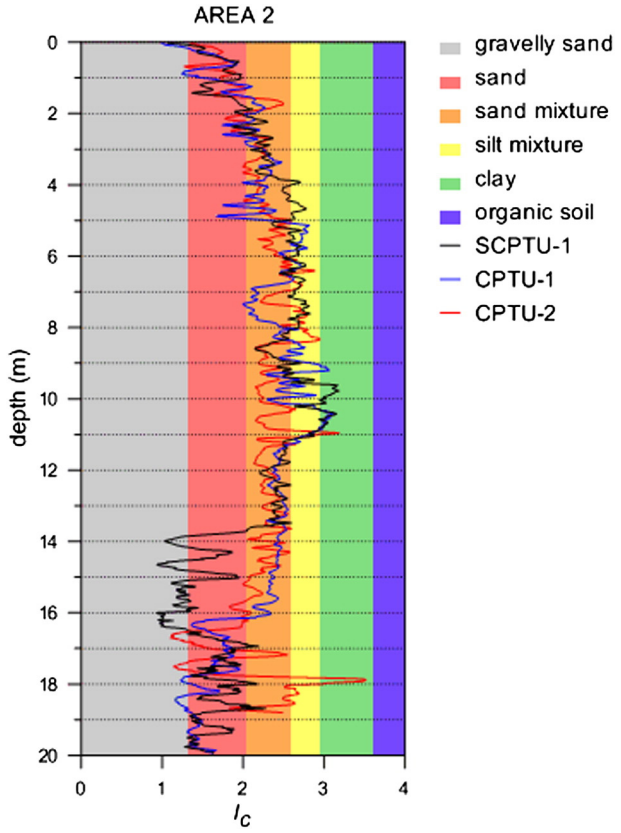

Fig. 9. Continuous profile of Soil Behavior Type index (I_c) calculated from CPTU data in Area 2. Superposition of three tests performed a few hundred meters apart shows the spatial variability of the stratigraphy.

It must be emphasized that the values obtained by FDEM measurements represent a weighted average of electrical resistivity in the top 6 m, thus we cannot expect from FDEM a detailed soil profile as given by ERT. The advantage of FDEM lies, obviously, in the ease of acquisition that allows a rapid screening of very long embankment stretches. In the present case study the comparison between FDEM and ERT was part of the project goals and this comparison proved largely satisfactory (see Results and discussion section).

For GPR acquisitions we used two different systems: a PulseEKKO-Pro by Sensor & Software Inc. with 50 MHz antennas and the dual frequency Hi-Mod GPR System by IDS Instruments with 200–600 MHz antennas. Here, like for FDEM, we present the results as separate lines: four continuous acquisitions labeled from GPR1 to GPR4 in Area 1 and seven continuous acquisitions labeled from GPR5 to GPR11 in Area 2 (Fig. 5). GPR data processing was fairly standard, including a static correction, a mean-subtraction dewow, a background removal and a manual gain, all performed using REFLEX™ by Sandmeier Scientific Software (www.sandmeier-geo.de).

3. Results and discussions

3.1. Geotechnical investigation

Grain size analyses were performed on samples selected every meter from the borehole cores, thus providing a detailed profile of the soil grain size versus depth. Fig. 6 shows the distribution (as %) of the grain size classes from 0 to 20 m along the two boreholes. Visual observation of the borehole cores, supported by grain size analyses, shows the following features:

- in Area 1 (borehole B-2, Fig. 6b) a 7 m layer of sandy silt overlies a 5 m layer of clayey silt/silty clay, followed by a 5 m layer of silty sand and finally a layer of medium gravel with sand that extends down to the bottom of the borehole.
- in Area 2 (borehole B-1, Fig. 6a) a 2 m layer of very sandy silt overlies a 9 m thick layer of silt with variable percentages of sand and clay; below, a thin layer of silty clay is present between 11 and 12 m, that overlays a 2 m thick deposit of sandy silt; from 14 m to the bottom of the borehole we find medium gravel with sand.

During borehole drilling, at both test sites, the water table was detected at about 10 m below the levee crest.

The results of the SCPTU tests are shown in Fig. 7 in terms of corrected cone tip resistance (q_t, in MPa), sleeve friction (f_s, in MPa), porewater pressure (u_2, in MPa) and shear wave velocity (V_s in m/s). The ratio between sleeve friction and cone tip resistance – called friction ratio ($R_f = 100\, f_s/q_t$) – is also shown. Data recorded in SCPTU-1 show a cone resistance lower than 2 MPa only for a thin layer around 10 m depth. At the same depth the pore water pressure increases thus confirming the presence of a clayey (low permeability) layer. A cone resistance between 4 and 6 MPa is measured in correspondence of the sandy silt layer found in borehole B-1 between 12 and 14 m from the embankment crest. A cone resistance higher than 6 MPa and highly fluctuating is recorded in the shallow sandy layer (0–2 m) and in the gravelly layer below 14 m.

Superposition of the I_c profiles for the three penetration tests executed in the Area 2 highlights some spatial variability in the stratigraphic profile (Figs. 8 and 9). The clayey layer detected at 10 m in SCPTU-1 (and B-1) is practically absent in CPTU2. The gravel layer starts at 14 m in SCPTU-1 (and B-1) and 16 m in CPTU-1 and CPTU-2. The detected variations are important in the geotechnical design. The presence of a clayey impervious layer that can act as a separator between two aquifers as well as the position of a highly permeable gravelly layer are key features to take into account in the definition of the stratigraphic model to adopt in a seepage analysis. The less favorable soil profile should be adopted for the calculations.

3.2. ERT surveys

Meaningful samples of the ERT results are shown in Figs. 10 to 13. The sections are presented in the $\log_{10}$ resistivity scale, where resistivity is in Ω m. The values of log-resistivity range between 1 and 3, i.e. they span two orders of magnitude. In particular the ERT images show, in both Areas 1 and 2, a more resistive shallow layer resting upon a more conductive material at depth. Specifically:

- in Area 1, the longitudinal and transverse ERT2 and ERT3 profiles (Figs. 10 and 11), show the presence of a shallow layer with log-resistivity values $\rho > 2.2$ down to a depth of about 6 m. Note that the transverse profiles, having a finer resolution than the longitudinal ones, show in much more detail the spatial variability even within this higher resistivity layer.
- in Area 2, along the longitudinal and transverse ERT6 and ERT7 profiles (Figs. 12 and 13), the presence of a shallow layer characterized by relatively high values of $\log_{10}$ resistivity ($\rho > 2.2$ Ω m) between the levee top of and about 3 m in depth and an area characterized by relatively low values of $\log_{10}$ resistivity ($\rho < 2.2$ Ω m) at depths greater than 3 m from the ground surface. Here too the transverse profiles offer a much more detailed picture.

A direct comparison of geo-electrical results and geotechnical data shows how:

- the layer characterized by high resistivity values in the top few meters of depth in Area 1 is well correlated to the 7 m layer (between 0 and 7 m from ground surface) of sandy silt that is visible at the top of the B-2 borehole (see Fig. 6b); the deep area with the lowest resistivity values is related to the 5 m layer (between 7 and 12 m from ground surface) of clayey silt/silty clay.

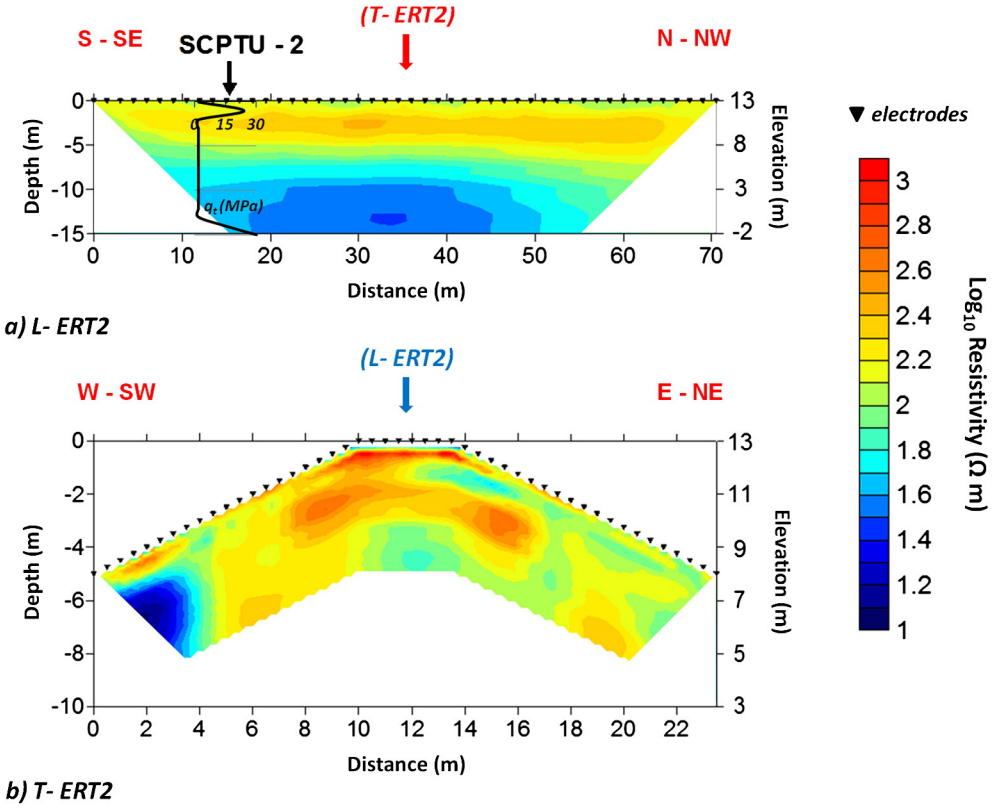

Fig. 10. Inversion results obtained from L-ERT2 and T-ERT2 surveys (Area 1). The values of electrical resistivity (in Ω m) are plotted on a logarithmic scale. The left vertical axis indicates depth (in m) from the ground surface (top of the levee); the right vertical axis indicates elevation above mean sea level (in m). The black arrow indicates the location of the SCPTU-2 test along the ERT profile. The simplified SCPTU results – in terms of corrected cone tip resistance (q_t, in MPa) – are superimposed over the ERT section. The point of intersection between the profiles is also indicated. Note the presence of a shallow layer with log-resistivity values $\rho > 2.2$ down to a depth of about 6 m. Due to their finer resolution, the transverse profiles offer a much more detailed picture with respect to the longitudinal ones.

- the layer characterized by high resistivity values in the first meters of depth in the Area 2 is well correlated with the 2 m layer (between 0 and 2 m from ground surface) of very sandy silt that overlies the 9 m thick layer of silt with variable percentage of sand and clay along the B-1 borehole (see Fig. 6a); this second layer, placed between 2 and 11 m from ground surface, is related to the deep area characterized by the lowest resistivity values along the ERT profiles.

The ERT lines longitudinal to the embankment, albeit not theoretically robust in terms of 2D resistivity inversion (as discussed above), allow for a non-invasive verification of the longitudinal continuity of the layers (albeit with some smooth variation along the profiles — see also our discussion of FDEM results below) as identified by borehole cores and confirmed by the still scattered CPTU and SCPTU surveys:

- high cone tip resistance values ($q_c \geq 4$ MPa) and shear wave velocities ($V_s > 200$ m/s) in correspondence of the layers with the highest percentage of sand and hence the highest electrical resistivity;
- low cone tip resistance values ($q_c < 4.0$ MPa) and shear wave velocities ($V_s \approx 200$ m/s) are, instead, well correlated to the more conductive layers, which are characterized by the highest percentage of fine materials (silts and sandy silts).

The SCPTU-1 profile (see Fig. 7), for example, highlighted the presence of a first layer (between 0 and 2 m in depth) with q_c values greater than 6.0 MPa and V_s greater than 200 m/s and a second layer (between 2 and 11 m in depth) with q_c values equal to 3.0 MPa and V_s equal to 200 m/s, which are strongly related to the results obtained along lines L-ERT7 and T-ERT7 sections (see Fig. 13).

Note also that, while the longitudinal lines show a general continuity (consider Figs. 10a, 11a, 12a, 13a) allowing the extrapolation of the few geotechnical data points along the axis of the embankment, the transverse lines show the fine scale details related possibly to different construction phases, possibly following failures or as measures of reinforcement. E.g. line T-ERT6 shows the presence of a deeper conductive layer also in the embankment flank to the North-East (i.e. towards the river) that is in continuity with the core of the embankment. The anomalous cross-section of the embankment in this area may indicate a collapse with reconstruction of the top part with more sandy material. A number of local anomalies can be highlighted in the transverse ERT lines. See e.g. the different configuration of the profile in line T-ERT7, where the south-western flank – towards inland – also shows a bulge that is made of silty-sand, and possibly constructed to block water seepage from below the embankment.

3.3. FDEM surveys

The results of FDEM surveys in Area 1 and Area 2 are shown in Figs. 14 and 15 respectively. Note that, given the used measurement device, the resistivity values can be considered as “apparent” or bulk resistivity values pertaining to the top 6 m below ground, i.e. practically to the whole body of the embankment. Proceeding from South to North along the levee system of Area 1, in particular, it is possible to note (see Fig. 14):

- a progressive slight decrease in the values of $\log_{10}$ resistivity along the FDEM1 profile, between a maximum value of about 2.1 and a minimum value of 1.8 (i.e. from about 125 Ω m to about 63 Ω m, i.e. of a factor 2);
- an increase in the values of electrical resistivity along the FDEM2 profile, from a minimum value of approximately 1.8 up to a maximum

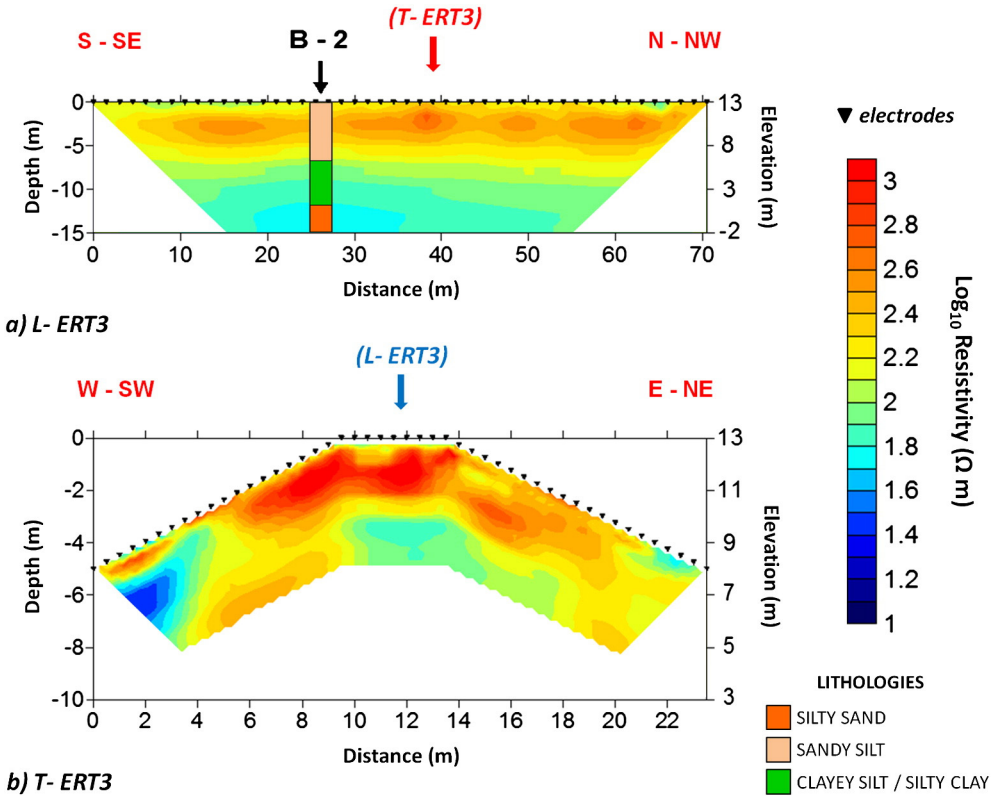

Fig. 11. Inversion results obtained from the L-ERT3 and T-ERT3 (Area 1). The values of electrical resistivity (in Ω m) are plotted on a logarithmic scale. The left vertical axis indicates depth (in m) from the ground surface (top of the levee); the right vertical axis indicates elevation above mean sea level (in m). The black arrow indicates the location of the B-2 borehole along the ERT profile. The simplified borehole results are superimposed over the ERT section. The point of intersection between the profiles is also indicated. Note the presence of a shallow layer with log-resistivity values ρ > 2.2 down to a depth of about 6 m. Due to their finer resolution, the transverse profiles offer a much more detailed picture with respect to the longitudinal ones.

value of 2.1; in practice the two profiles FDEM1 and FDEM2 show jointly a minimum of resistivity around their connection point (see map in Fig. 4);
- a nearly constant value of $\log_{10}$ resistivity of about 2.0–2.1 m along the FDEM3 and FDEM4 profiles;
- out of scale values due to the presence of a buried metallic pipe along the FDEM3 profile, at 35–40 m of distance from its starting point; the identification of this feature is very important for the assessment of failure risk in this area, as pipes shall not cross, obviously, the embankment structure.

The slight variation in electrical resistivity values is obviously related to changes in the thickness of the first layer detected in the subsurface of Area 1, which is characterized by the highest resistivity values as shown in the ERT longitudinal profiles. A relative increase in electrical resistivity values is, for example, shown in the top 6 m of section L-ERT 2 (see Fig. 10a), which corresponds to the trend highlighted by the FDEM2 profile; the nearly constant value of $\log_{10}$ resistivity of about 2.0–2.1 along the FDEM3 profile is also well correlated with the results in the L-ERT3 line (see Fig. 11a).

Similar considerations that can be made are deductible from the analysis and comparison of the acquisitions in Area 2 (see Fig. 15). Note, for example:

- a slight, progressive increase in the values of $\log_{10}$ resistivity along the FDEM5 and FDEM6 profiles, from a minimum value of approximately 1.9 Ω m up to a maximum value of 2 Ω m;
- a nearly constant value of $\log_{10}$ resistivity of about 1.9 along the FDEM7 to FDEM10 profiles;
- out of scale values along FDEM7 due to the presence of a buried metallic pipe, at around 10–15 m of distance from the starting point — here too like in Area 1 the presence of this pipe may produce weakness in the embankment structural or hydraulic capabilities;
- a general decrease in the values of electrical resistivity along the FDEM11 profile.

The nearly constant average value of the electrical resistivity measured along the levee system in the Area 2 is strongly correlated to the layer succession that has been detected by the in-situ geotechnical tests and the ERT surveys; in particular, FDEM measurements are influenced by the presence of the 2 m layer of very sandy silt (characterized by high resistivity values — see Figs. 12 and 13) and the 9 m thick layer of silt with sand and clay (characterized by lower resistivity values) that are visible along the B-1 borehole log (see Fig. 6a). As in Area 1 the slight variation in electrical resistivity values highlighted by the FDEM profiles is obviously related to changes in the thickness of the first layers detected in the subsurface.

3.4. GPR surveys

Some of the most meaningful results obtained at different frequencies (50, 200 and 600 MHz) are shown in Figs. 16 to 19. We took into account a signal propagation speed of about 0.08 m/ns, as resulted from velocity analysis applying hyperbola fitting (a localized object – a metallic pipe, in this case – produced a hyperbola on the records, which was important for the determination of the radar velocity).

Before the results' analysis, it is necessary to make careful considerations regarding the penetration and resolution for each of the frequencies used. In particular: the acquisitions made at the lowest frequency (50 MHz, with a wavelength equal to roughly 1.6 m) ensured a greater penetration, but of course a much lower resolution with respect to the surveys conducted with higher frequencies; the acquisition made at a frequency of 200 MHz (and a wavelength roughly equal to 0.4 m) allowed an intermediate penetration and a theoretical resolution equal to 0.1 m; the acquisition at a frequency of 600 MHz gave very

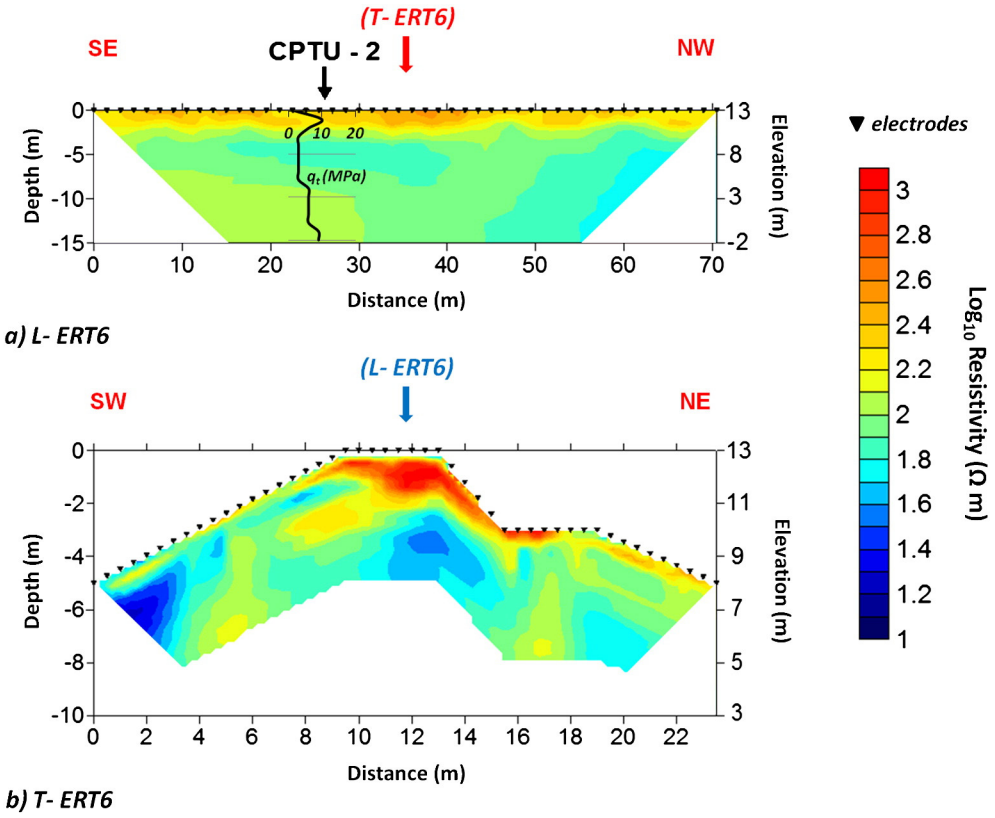

Fig. 12. Inversion results obtained from the L-ERT6 and T-ERT6 surveys (Area 2). The values of electrical resistivity (in Ω m) are plotted on a logarithmic scale. The left vertical axis indicates depth (in m) from the ground surface (top of the levee); the right vertical axis indicates elevation above mean sea level (in m). The black arrow indicates the location of the CPTU-2 test along the ERT profile. The simplified CPTU results – in terms of corrected cone tip resistance (q_t, in MPa) – are superimposed over the ERT section. The point of intersection between the profiles is also indicated. Note the presence of a shallow layer with log-resistivity values ρ > 2.2 down to a depth of about 3 m. Due to their finer resolution, the transverse profiles offer a much more detailed picture with respect to the longitudinal ones.

high resolution images (the wavelength is roughly 0.13 m), but with a very small penetration.

In summary, the 50 MHz survey allowed a maximum penetration which, given the relatively large electrical conductivity of the embankment material, does not exceed 2 m from the embankment crest. The 200 MHz and 600 MHz surveys practically penetrate the same depth, with much better resolution.

The GPR results related to Area 1 are shown in Figs. 16 and 17. In particular, the acquisitions at 50, 200 and 600 MHz along line GPR2 are in Fig. 16: the radargrams cover about 200 m and reveal the presence of very shallow highly discontinuous reflectors at depths between 0.5 and 2 m from the ground surface. The structural details are highlighted better by the higher frequencies. As previously mentioned, the signal penetration does not exceed 2 m. The strong attenuation of the GPR signal during wave propagation in the subsurface is due to the presence of fine materials below this depth range. As previously mentioned, in fact, borehole logging performed along the embankment has identified a succession of sandy silt and clayey silt/silty clay in Area 1 (see Fig. 6b).

Similar results have been obtained for the other GPR lines in Area 1. Note, for example, in GPR3 the presence of some reflectors placed at depths between 0.5 and 2 m from ground surface (Fig. 17). In this figure it is also apparent the shallow diffraction (at about 1 m depth) caused by the metallic pipe discussed above for the FDEM results. Note however that this pipe is visible in the GPR images only because the pipe is indeed at very shallow depth. Should it be placed below 2 m from the crest, this anomaly would be invisible to GPR while still detectable by FDEM.

Similar considerations about the depth of investigation and resolution are valid also for Area 2 (Figs. 18 and 19). In particular, the presence of some reflectors is apparent between 0.5 and 2 m from ground surface. Here too the strong attenuation of GPR signal in the silty subsoil prevents the depth of penetration from exceeding 2 m from the ground surface. The 2 m thick layer of sand with silt that has been collected between 0 and 2 m from ground surface in the Area 2 overlies, in fact, a thick layer of sandy silt that extends up to 14 m in depth (Fig. 6a).

As the reference depths are significantly different, in the specific case it is impossible to compare the data that have been obtained by GPR radargrams with the data that have been derived from borehole logs and CPTU and SCPTU tests, if exception is made for the topmost, electrically conductive silty layer that attenuates the GPR signal and limits its depth of penetration.

4. Conclusions and outlook

The geophysical characterization conducted at the pilot site of San Michele al Tagliamento allowed us to obtain important information on the internal characteristics of the Tagliamento River embankments, covering in a short time large portions of the system with a meter resolution. As shown in the Results and discussion section, the comparison with direct (invasive) techniques, and, more particularly, with CPTU/SCPTU results was fundamental for a proper calibration of the results. With regard to the different investigation methods, it was possible to highlight:

1. the high resolution capabilities of the electrical resistivity tomography, in particular of the transverse ERT sections, which clearly show the layers sequence at depth, from the top to the bottom of the embankments, and below. This differentiation (in terms of electrical characteristics) in the first meters of the subsurface, due to differences in lithology and water content, is similar in all sections of *Area 1* and while it is diversified along the embankment of *Area 2*;

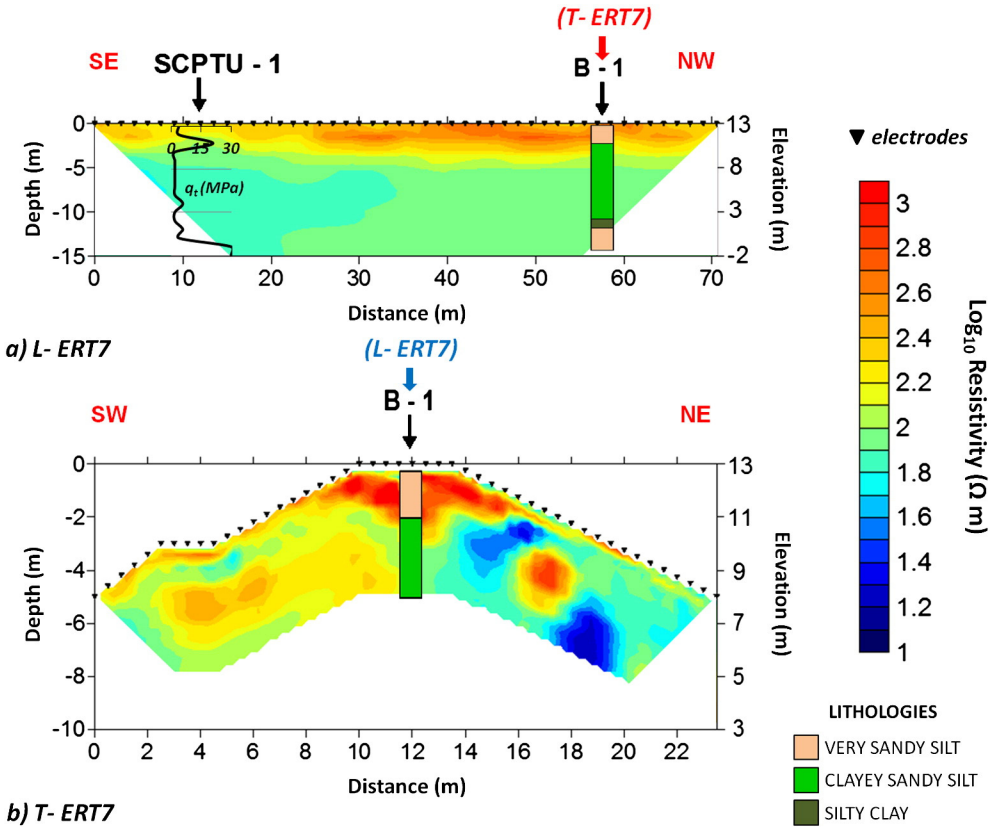

Fig. 13. Inversion results obtained from the L-ERT7 and T-ERT7 surveys (Area 2). The values of electrical resistivity (in Ω m) are plotted on a logarithmic scale. The left vertical axis indicates depth (in m) from the ground surface (top of the levee); the right vertical axis indicates elevation above mean sea level (in m). The black arrows indicate the location of the B-1 borehole and SCPTU-1 test along the ERT profile. The simplified borehole and SCPTU results – in terms of corrected cone tip resistance (q_t, in MPa) – are superimposed over the ERT section. The point of intersection between the profiles is also indicated. Note the presence of a shallow layer with log-resistivity values ρ > 2.2 down to a depth of about 3 m. Due to their finer resolution, the transverse profiles offer a much more detailed picture with respect to the longitudinal ones.

2. the great potential of the electromagnetic method in the frequency domain, the results of which are well correlated to those obtained with the electrical resistivity tomography, providing a fast characterization of the first meters in the subsurface (down to about 6 m from the levee crest) covering the entire embankment height. The downside is that FDEM provides only a bulk resistivity value for the investigated volume and of course lacks the resolution of ERT. Note however that FDEM detected the presence of a buried metal pipe, not seen in the ERT measurements;
3. the limited resolution capabilities of the Ground Penetrating Radar technique, which, despite being considered often the method of choice for fast embankment characterization, in this case GPR did not provide any information at depths greater than 2 m from the ground surface, thus covering only the top one third of the embankment height. The presence of fine-grained materials (mainly composed of sandy silt and silt), in fact, led to a strong attenuation of the signal and severely limited the resolution capabilities. But the presence of fine material in embankments is more the rule than an exception. Therefore it must be expected that the presence of shallow, fine grained and electrically conductive layers may screen the remaining embankment structure from GPR investigation, not revealing indeed much about the grain size below or the presence of animal burrows, so often presented as a danger for embankments that lend itself to fast and reliable GPR identification. More reliable results may be obtained with redundant information, using a grid-like acquisition (e.g. Kinlaw, and Grasmueck, 2012). In our study, the GPR confirmed the presence of metallic pipe already highlighted by the FDEM method, but only because this pipe is very shallow (1 m depth) and rests in the resistive layer on top of the embankment itself.

In summary, the integration of different geophysical survey techniques, with proper calibration to geotechnical data, allowed us to identify areas with different structural characteristics and to underline the advantages and disadvantages of each of the methodologies used in the specific context. Note, however, that the application of GPR proved rather disappointing. The identification of voids and cavities created, for example, by animals, does not seem reliable using GPR, especially when used on electrically conductive structures (rich in fine materials, such as silts and clays) such as those that commonly compose river embankments. The geophysical techniques used in this first stage of static (geometric) characterization of river embankment could also provide estimates of the change in system parameters (in particular of the water content) and hence a dynamic characterization of the levees using time-lapse acquisitions. The changes in water content may have destabilizing effects on the levee structure, so an effective monitoring in time and space would allow to locate the most vulnerable areas. Especially with ERT surveys, it would be possible to create 2D and/or 3D maps of water content, with location of preferential flow paths. Time-lapse results can be translated into quantitative estimates of the variables involved into calibration of the constitutive relationships for laboratory experiments. Therefore, it would be preferable for the future to repeat such application over time (in time-lapse mode). To this end, fast means of conductive ERT surveys by means of towed systems would prove extremely useful to speed up acquisition and allow for the detailed embankment characterization that ERT can provide, and that cannot be achieved with either FDEM or GPR. Anyhow, detailed images of the subsurface can be provided by traditional ERT methods once they are focused in areas of anomalous signal produced e.g. by the much faster FDEM approach.

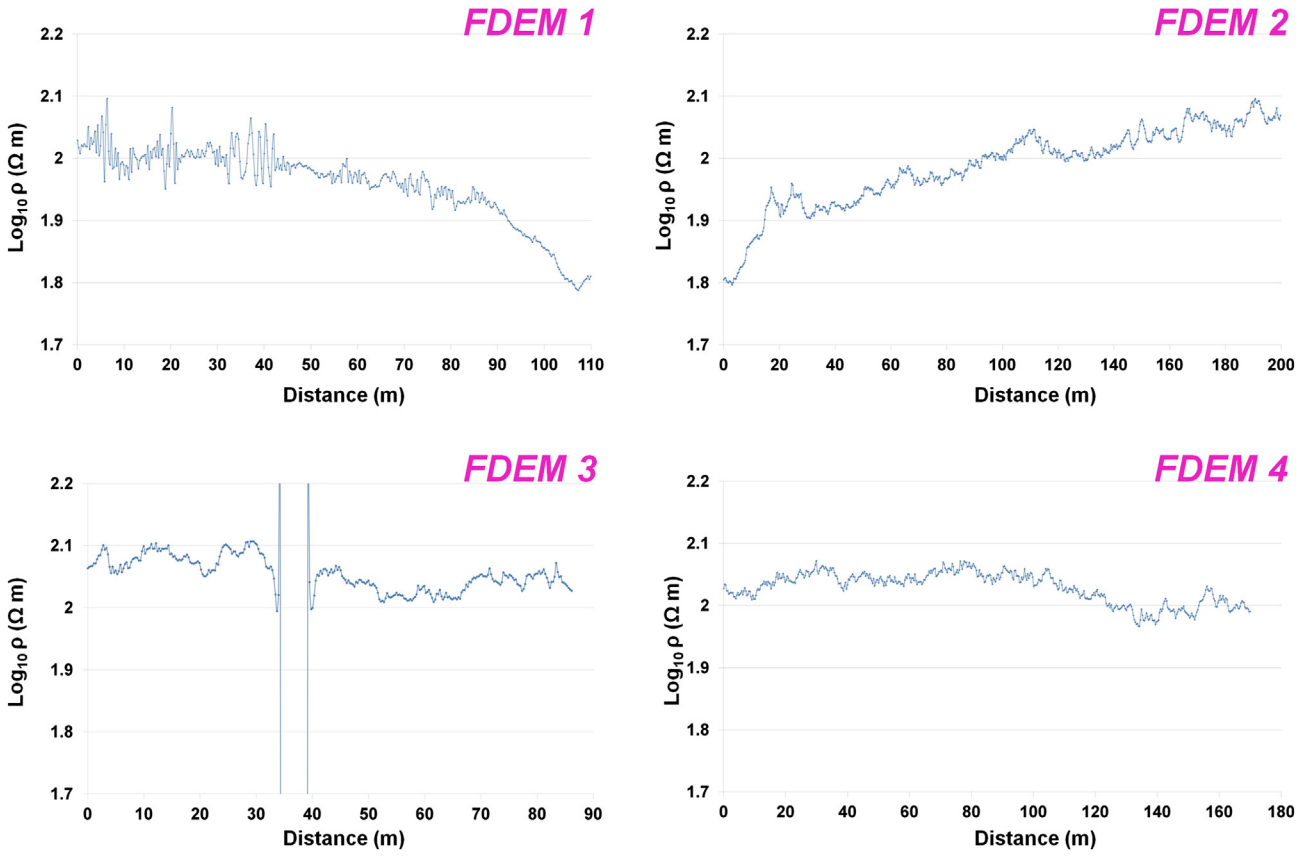

Fig. 14. FDEM results obtained along the levee system in Area 1. The values are expressed in terms of $\log_{10}$ resistivity (in Ω m).

Other possible future developments should involve also the realization of larger-scale non-invasive measurements, able to detect the subsoil configuration under the embankments, as groundwater seepage that may occur below these structures can play a major role in their stability, as much as the structure of the embankments themselves.

Acknowledgments

The authors wish to acknowledge the support from the "Genio Civile" office in Venice, that has kindly given the permission to use the data published in this study.

References

Begemann, H.K.S., 1965. The friction jacket cone as an aid in determining the soil profile. Proceedings of the 6th International Conference on Soil Mechanics and Foundation Engineering, ICSMFE, 2, 17–20, Montreal, September 8.

Biavati, G., Ghirotti, M., Mazzini, E., Mori, G., Todini, E., 2008. The use of GPR for the detection of non-homogeneities in the Reno River embankments (North-Eastern Italy). 4th Canadian Conference on Geohazards: From Causes to Management. Université Laval, Québec: Canada, pp. 20–24.

Buselli, G., Lu, K., 2001. Groundwater contamination monitoring with multichannel electrical and electromagnetic methods. J. Appl. Geophys. 48, 11–23.

Cho, I., Yeom, J., 2007. Crossline resistivity tomography for the delineation of anomalous seepage pathways in an embankment dam. Geophysics 72, G31–G38.

Cortellazzo, G., Simonini, P., 2001. Permeability evaluation in modeling the consolidation of an Italian soft clay deposit. Can. Geotech. J. 38, 1166–1176.

Daily, W., Ramirez, A., Binley, A.M., LaBrecque, D., 2004. Electrical resistivity tomography. Lead. Edge 23 (5), 438–442.

Di Prinzio, M., Bittelli, M., Castellarin, A., Rossi Pisa, P., 2010. Application of GPR to the monitoring of river embankments. J. Appl. Geophys. 71 (2–3), 53–61 (June).

Fauchard, C., Meriaux, P., 2007. Geophysical and Geotechnical Methods for Diagnosing Flood Protection Dikes. Editions Quae, Paris (197 pp.).

Fontana, A., Bondesan, A., Meneghel, M., Toffoletto, F., Vitturi, A., Bassan, V., 2012. Note Illustrative della Carta Geologica d'Italia 1:50.000 - Foglio 107 Portogruaro, Regione Veneto, InfoCartoGrafica, Piacenza.

Inazaki, T., 2007. Integrated geophysical investigation for the vulnerability assessment of earthen levee. SAGEEP 2007, Symposium on the Application of Geophysics to Enginering and Environmental Problems.

Kinlaw, A., Grasmueck, M., 2012. Evidence for and geomorphologic consequences of a reptilian ecosystem engineer: the burrowing cascade initiated by the Gopher Tortoise. Geomorphology 157–158, 108–121. http://dx.doi.org/10.1016/j.geomorph.2011.06.030.

LaBrecque, D.J., Miletto, M., Daily, W., Ramirez, A., Owen, E., 1996. The effects of noise on Occam's inversion of resistivity tomography data. Geophysics 61, 538–548. http://dx.doi.org/10.1190/1.1443980.

Niederleithinger, E., Weller, A., Lewis, R., 2012. Evaluation of geophysical techniques for dike inspection. J. Environ. Eng. Geophys. 17 (4), 185–195.

Panthulu, T.V., Krishnaiah, C., Shirke, J.M., 2001. Detection of seepage paths in earth dams using self-potential and electrical resistivity methods. Eng. Geol. 59, 281–295.

Reynolds, J.M., 2011. An Introduction to Applied and Environmental Geophysics. John Wiley & Sons Ltd, (696 pp.).

Robertson, P.K., 1990. Soil classification using the cone penetration test. Can. Geotech. J. 27 (1), 151–158.

Robertson, P.K., 2009. Interpretation of cone penetration test—a unified approach. Can. Geotech. J. 46, 1337–1355.

Robertson, P.K., 2012. Interpretation of in-situ tests: some insights. Geotechnical and Geophysical Site Characterization 4 — Mitchell Lecture. Taylor & Francis Group, London.

Szynkiewicz, A., 2000. GPR monitoring of earthen flood banks/levees. Eighth International Conference on Ground Penetrating Radar. Proc. of SPIE. vol. 4084, pp. 85–90.

Tanaka, H., Tanaka, M., Iguchi, H., Nishida, K., 1994. Shear modulus of soft clay measured by various kinds of tests. Proceedings of the International Symposium on Pre-failure deformation of Geomaterials. Balkema, Rotterdam, pp. 235–240.

Teh, C.I., Houlsby, G.T., 1991. An analytical study of the cone penetration test in clay. Geotechnique 41, 17–34.

Tockner, K., Ward, J.V., Arscott, D.B., Edwards, P.J., Kollmann, J., Gurnell, A.M., Petts, G.E., Maiolini, B., 2003. The Tagliamento River: a model ecosystem of European importance. Aquat. Sci. 65, 239–253.

Torstensson, B.A., 1975. Pore pressure sounding instrument. Proc. A. Soc. Civ. Engrs. Spec. Conf. In situ measurements of soil properties. 2, pp. 48–54.

Voronkov, O.K., Kagan, A.A., Krivonogova, N.F., Glagovsky, V.B., Prokopovich, V.S., 2004. Geophysical methods and identification of embankment dam parameters. Procs. 2nd International Conference on Site Characterization (ISC), Porto, Portugal, 19–22 September, pp. 593–599.

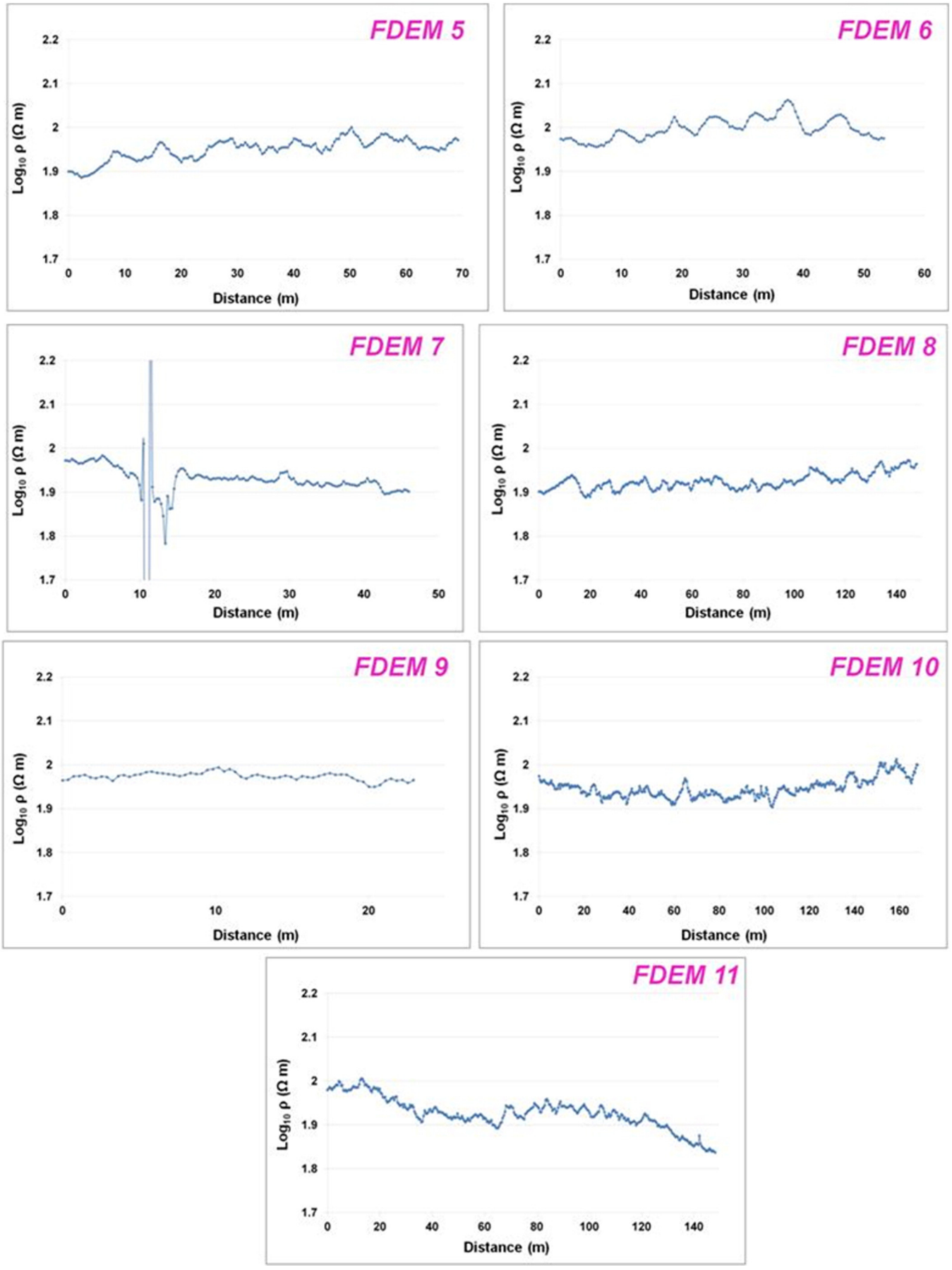

Fig. 15. FDEM results obtained along the levee system in Area 2. The values are expressed in terms of $\log_{10}$ resistivity (in Ω m).

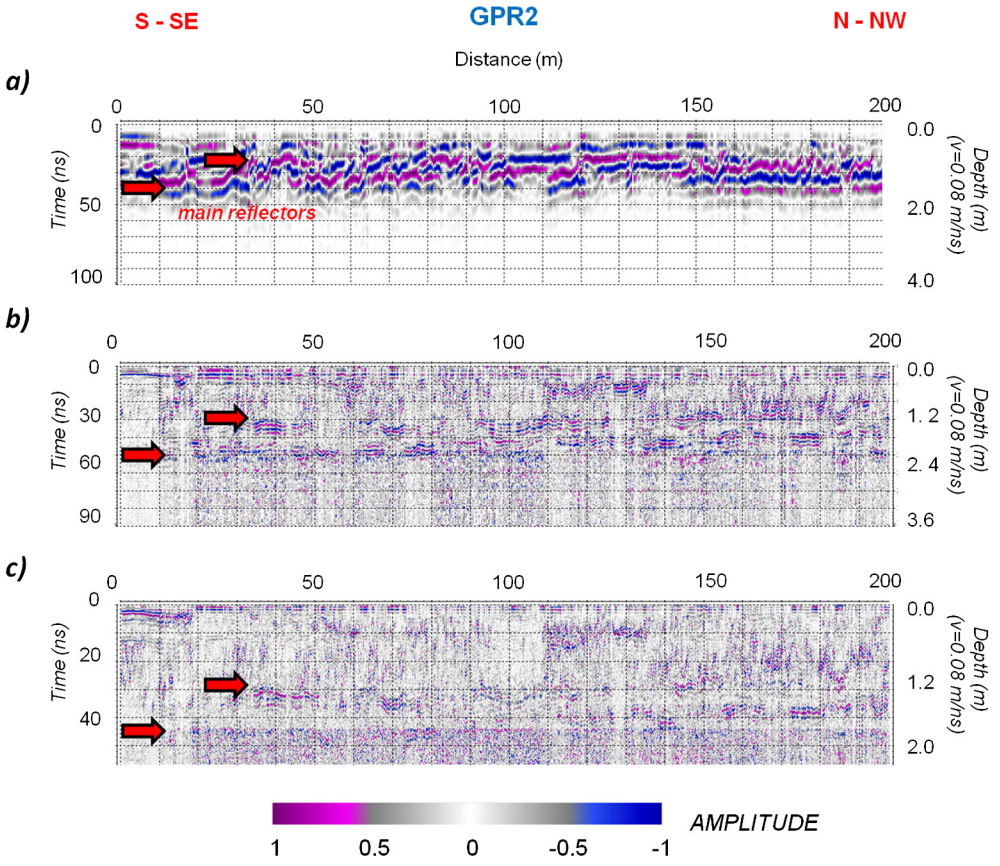

Fig. 16. Radargrams obtained along GPR2 line (Area 1) at 50 MHz (*a*), 200 MHz (*b*) and 600 MHz (*c*). The values of amplitude are shown with respect to time (in ns) and depth from the levee crest (in m, considering a velocity of 0.08 m/ns). The arrows indicate the depth at which the main reflectors lie.

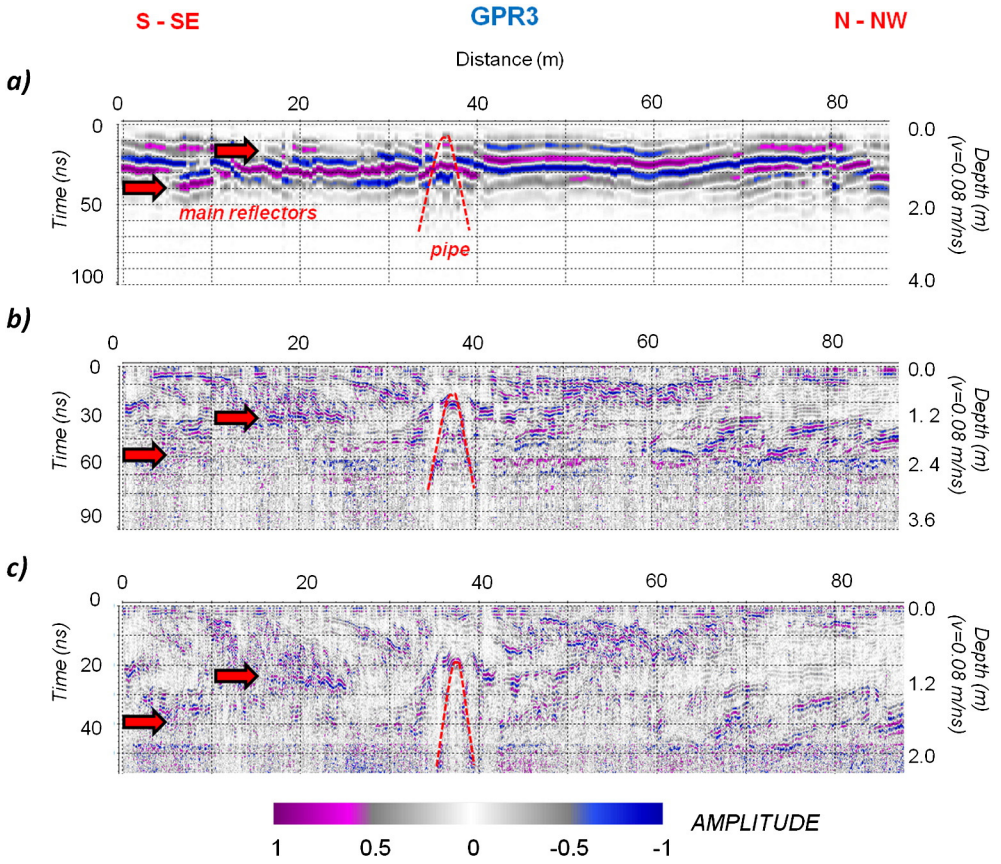

Fig. 17. Radargrams obtained along GPR3 line (Area 1) at 50 MHz (*a*), 200 MHz (*b*) and 600 MHz (*c*). The values of amplitude are shown with respect to time (in ns) and depth from the levee crest (in m, considering a velocity of 0.08 m/ns). The arrows indicate the depth at which the main reflectors lie. The hyperbola related to the presence of a buried metallic pipe is also highlighted (dashed curve).

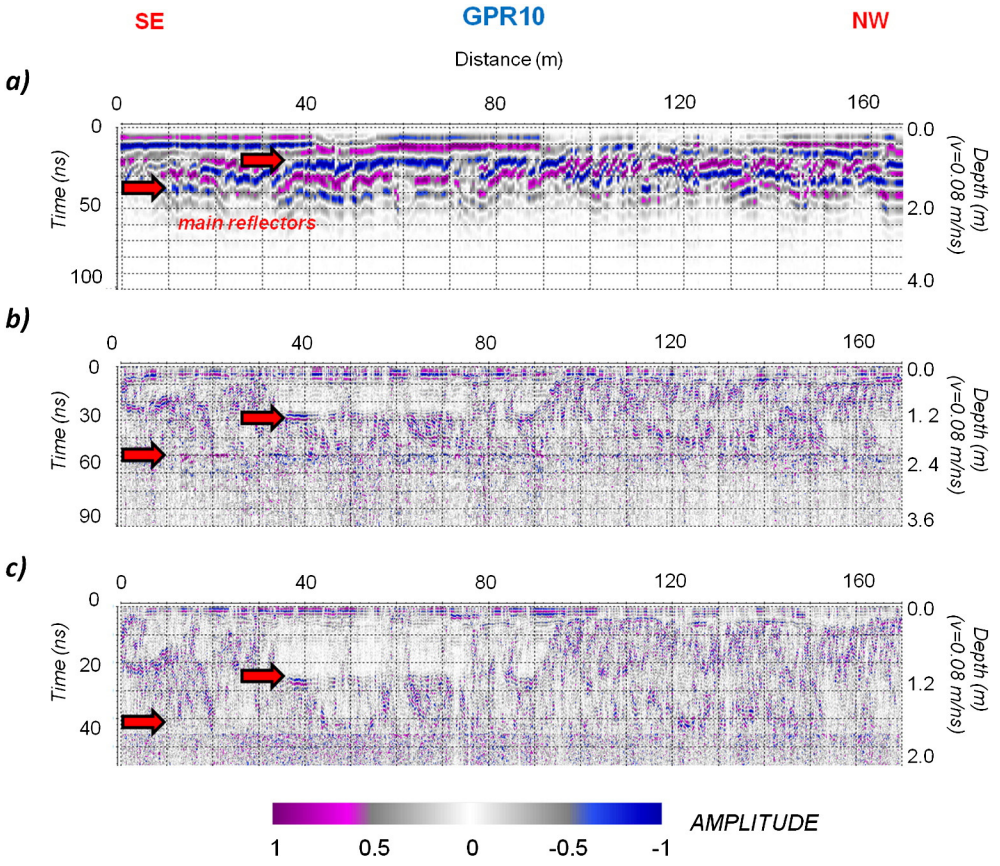

Fig. 18. Radargrams obtained along GPR10 line (Area 2) at 50 MHz (*a*), 200 MHz (*b*) and 600 MHz (*c*). The values of amplitude are shown with respect to time (in ns) and depth from the levee crest (in m, considering a velocity of 0.08 m/ns). The arrows indicate the depth at which the main reflectors lie.

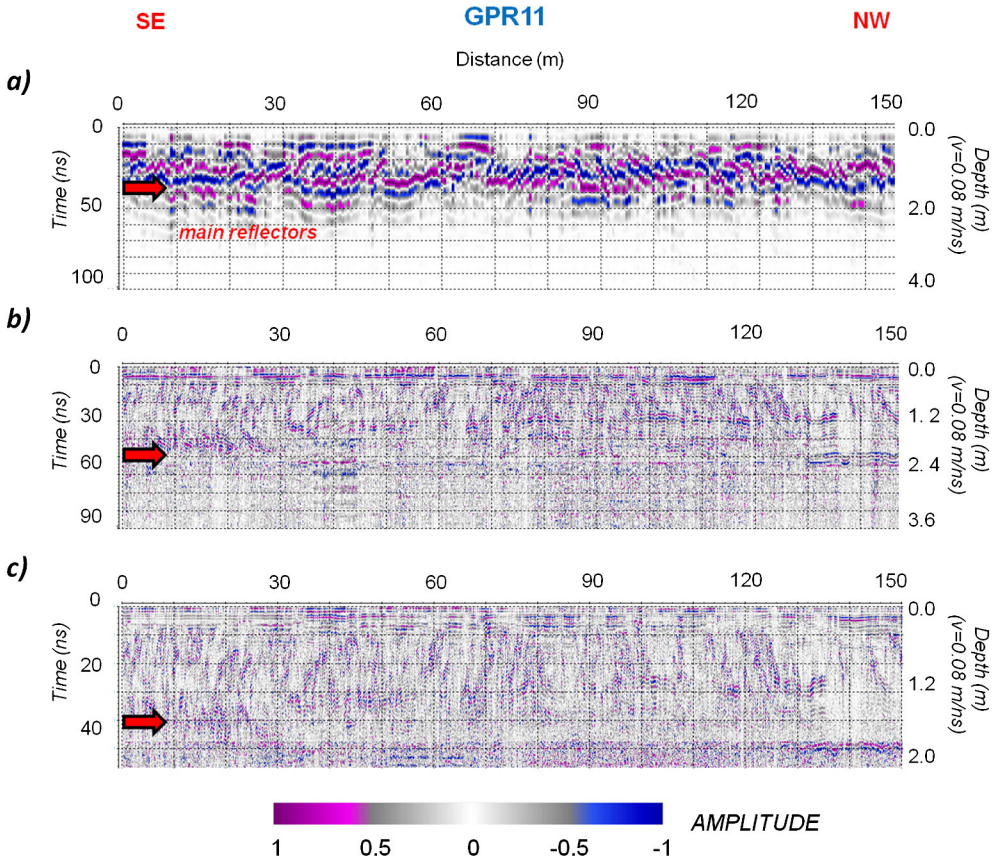

Fig. 19. Radargrams obtained along GPR11 line (Area 2) at 50 MHz (*a*), 200 MHz (*b*) and 600 MHz (*c*). The values of amplitude are shown with respect to time (in ns) and depth from the levee crest (in m, considering a velocity of 0.08 m/ns). The arrows indicate the depth at which the main reflectors lie.